exotherm. The absence of apparent osmotic driving force may explain the limited effect of storage at above the bulk solution freezing temperature.

The DPPC liposome suspensions extruded through larger pore size filters (e.g., 0.4 and 0.8 μm) showed larger intraliposomal solution freezing exotherms (Fig. 2a). Factors including the possibility of higher initial solution contents per lipid weight, limited membrane disordering associated with the curvature, and slower dehydration due to the increase in multilamellar membranes would explain the large exotherms. Liposomes composed of phosphatidylcholines of different acyl chain lengths showed retention of the intraliposomal solution down to the homogeneous ice formation temperature in the order of DMPC < DPPC < DSPC (Fig. 2b). The intraliposomal solution freezing exotherm was not observed in the thermal analysis of POPC liposome suspensions (data not shown). All the liposome membranes are below their T_m (POPC: −5°C, DMPC: 24°C, DPPC: 41°C, DSPC: 54°C) at the bulk solution freezing temperature.[35] Possible differences in the membrane fluidity and rigidity would cause the freeze-induced dehydration to vary.

Effect of Trehalose Distribution on Freezing Profiles of Liposome Suspensions

The effects of intra- and extraliposomal trehalose on the freezing behavior of liposome suspensions were studied. The DPPC liposome suspensions containing trehalose on both sides of the membrane showed larger intraliposomal solution peaks that suggest reduced solution loss upon the bulk solution freezing. For example, cooling of the 0.2 μm DPPC suspensions at 10°C/min resulted in exotherms of approximately 80 and 200 J/g lipid, respectively, in the absence and presence of trehalose (Figs. 2 and 4). The addition of trehalose also lowered the peak temperature of the exotherm (approx. 3°C at 12% trehalose, w/w).[18,34] The trehalose-containing liposome lost a larger amount of the internal supercooled solution during the slower cooling of the suspensions. Temporary pausing of the cooling scan suggested a faster loss of the supercooled solution near the bulk solution freezing temperature (−25°C), also in the trehalose-containing liposome suspensions (Fig. 3). The addition of various low-molecular-weight saccharides and polyols to both sides of the lipid membrane increased the freezing exotherm of the intraliposomal solutions, suggesting that slower freeze-induced dehydration occurred due to the colligatively determined osmotic effect (Fig. 5). The limited effect of dextran on the exotherm could be explained by its lower molar concentration and its possible exclusion from the vicinity of the liposomes in the freeze-concentrated non-ice phase.[36] The large (0.4 and 0.8 μm) or lower fluidity (DSPC) liposomes retained higher amounts of

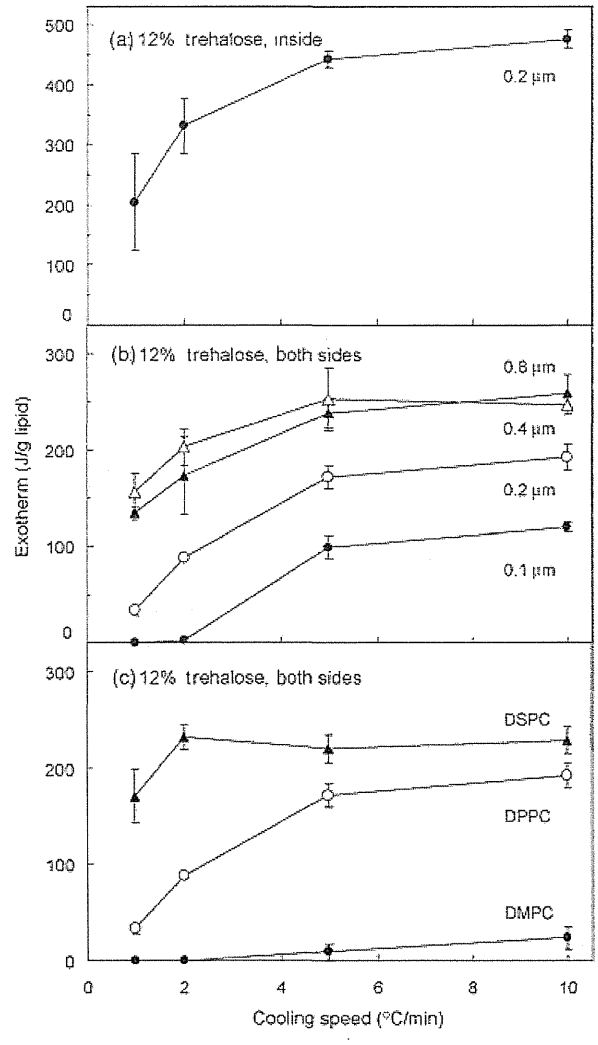

Figure 4. Internal solution freezing exotherms of liposome suspensions containing trehalose (12%, w/w) on (a) the inside and (b, c) both sides of liposomes. Aliquots of suspensions (10 μL, 4% lipid in 10 mM Tris–HCl buffer) containing liposomes with (b) differing extrusion membrane pore sizes (DPPC; 0.1 μm: •, 0.2 μm: ○, 0.4 μm: ▲, and 0.8 μm: △) and (c) lipid compositions (0.2 μm; DMPC: •, DPPC: ○, and DSPC: ▲) were cooled at 1–10°C/min (average ± SD, $n = 3$).

freezable intraliposomal solution in the presence of trehalose on both sides of the membrane (Figs. 4b and 4c).

1,2-Dipalmitoyl-*sn*-glycero-3-phosphocholine liposomes containing trehalose on one side of the membrane showed different freezing behaviors. The addition of higher concentration trehalose to the extraliposomal media reduced the intraliposomal solution freezing exotherm (Fig. 6). The difference in the osmotic pressures across the membrane should induce solution flow that dehydrates the liposomes both prior to cooling and after the bulk solution freezing. The

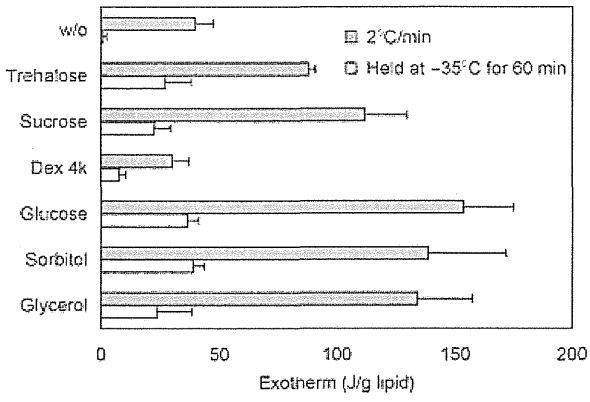

Figure 5. Effect of various extraliposomal solutes (12%, w/w) on internal solution freezing exotherms of DPPC liposome suspensions (10 μL, 4% lipid in 10 mM Tris–HCl buffer, 0.2 μm) obtained via cooling scans at 2°C/min (average ± SD, $n = 3$). Some suspensions were held at −35°C for 60 min during the scan.

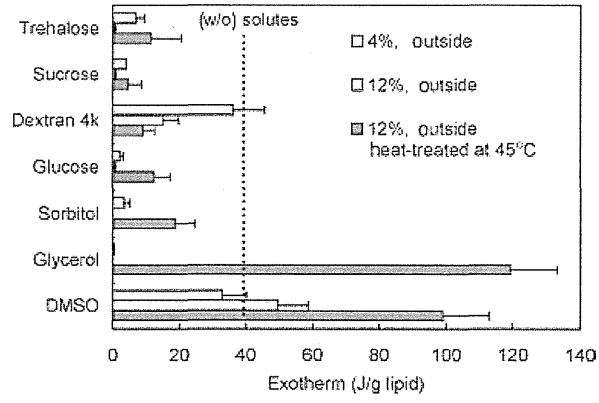

Figure 7. Effect of various extraliposomal solutes (4% and 12%, w/w) on internal solution freezing exotherms of DPPC liposomes obtained via cooling scans of suspensions (10 μL, 4% DPPC in 10 mM Tris–HCl buffer, 0.2 μm) from room temperature to −70°C at 2°C/min. Some suspensions were heat-treated at 45°C for 3 min before the cooling analysis (average ± SD, $n = 3$).

absence of a broad exotherm between the bulk and intraliposomal solution freezing peaks suggested that liposome dehydration before the bulk solution freezing (e.g., osmotic shrinkage) had occurred rather than the freeze-induced dehydration (data not shown).

Other low-molecular-weight saccharides and polyols in the extraliposomal media also reduced the intraliposomal solution freezing exotherms of the DPPC liposomes (Fig. 7). The extraliposomal dextran showed smaller effect to reduce the exotherm compared with the lower-molecular-weight excipients. Prior heat treatment of the liposome suspensions at above T_m of DPPC (45°C, 3 min), apparently increased the intraliposomal solution freezing exotherm of the suspensions containing the externally added glycerol or DMSO. Membrane disordering at and above the transition temperature should allow an influx of the highly permeable small solute molecules, and should, thus, reduce the osmotic effect that dehydrates the liposomes.

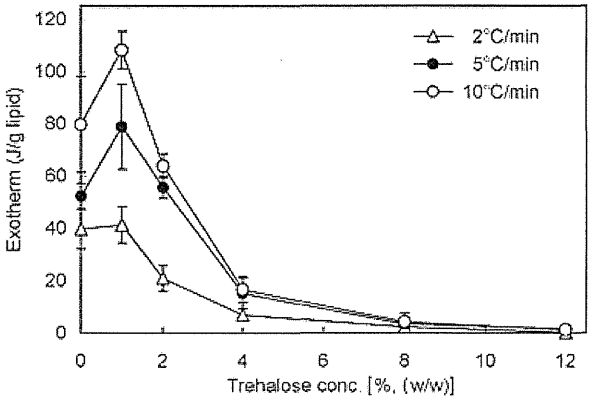

Figure 6. Effect of extraliposomal trehalose (0%–12%, w/w) on internal solution freezing exotherms of DPPC liposome suspensions (10 μL, 4% lipid in 10 mM Tris–HCl buffer, 0.2 μm) obtained by cooling at 2°C/min (Δ), 5°C/min (•), or 10°C/min (o)(average ± SD, $n = 3$).

The effect of intraliposomal trehalose on the freezing behavior of DPPC liposomes was also studied (Fig. 4a). The suspensions containing trehalose predominantly inside the liposomes showed apparently larger exotherms than those of other suspensions. The absence of the baseline shift at the trehalose transition temperature of maximally freeze-concentrated solutes (T_g') in the heating scan confirmed the low trehalose concentration outside the liposomes (data not shown). Liposomes prepared by extrusion often contain an amount of internal solution that was insufficient to fill the completely spherical structure, which allows inward water flow across the membrane upon exposure of liposomes to lower osmolarity solutions.[37] An increase in the intraliposomal solution content due to osmotic swelling in the initial suspension and limited freeze-induced dehydration can explain the larger ice formation peaks. These results indicated that the osmotic effect made a significant contribution to the freezing behavior of liposomes.

Kinetic stability of the trehalose-containing supercooled intraliposomal solutions was studied to elucidate their relevance in freeze-drying process (Fig. 8). Some liposome suspensions (e.g., trehalose-containing 0.8 μm DPPC liposome) showed small but apparent intraliposomal solution freezing peaks in the scans after a slower cooling (0.5°C/min) followed by being held at −35°C (180 min). The result suggested that some liposomes retain certain amount of internal solutions during freezing segment of pharmaceutical formulation lyophilization usually

DOI 10.1002/jps

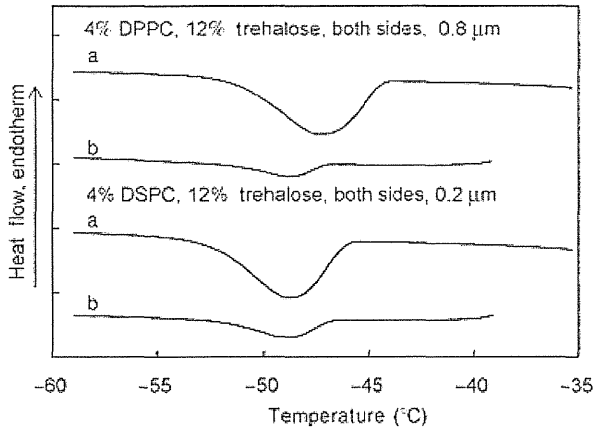

Figure 8. Cooling thermograms of DPPC (0.8 μm) and DSPC (0.2 μm) liposome suspensions containing trehalose (12%, w/w) on both sides of the membrane (10 μL, 4% lipids in 10 mM Tris–HCl buffer). The suspensions were cooled at 5°C/min (a) from room temperature or (b) after slow cooling (0.5°C/min) with a temporary pause at −35°C (180 min).

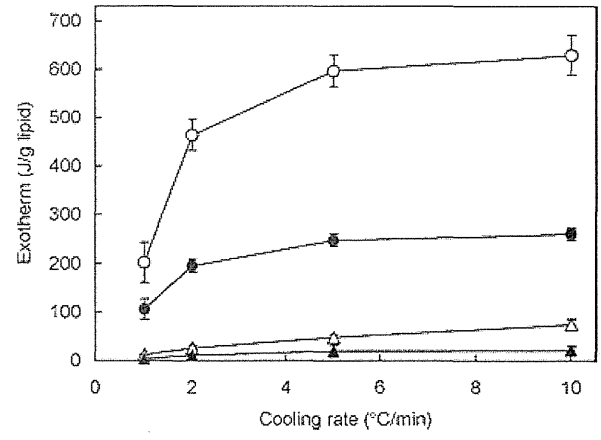

Figure 9. Internal solution freezing exotherms of carboxyfluorescein (25 mM)-containing DPPC liposome suspensions (10 μL, 4% DPPC in 10 mM Tris–HCl buffer, 0.2 μm) without (△) or with 12% trehalose on the outside (▲), inside (○), or both sides (●) of the liposome membrane scanned from room temperature at 1–10°C/min (average ± SD, $n = 3$).

performed via slow cooling (e.g., 0.2–0.5°C/min) down to −35°C to −50°C on the lyophilizer shelf.[38,39] The lower product temperature during the process should lead to freezing of the intraliposomal solutions by the homogeneous ice nucleation mechanism.

Effect of Freeze–Thawing on CF-Encapsulated Liposomes

The relationship between trehalose-induced changes in the liposome freezing behavior and functional stability of liposomes upon freeze–thawing was studied (Figs. 9 and 10). The CF-loaded DPPC liposomes were subjected to thermal analysis and freeze–thawing marker-retention study (a) without trehalose, (b) with trehalose on both sides of the membrane, (c) with trehalose in the intraliposomal solution, or (d) with trehalose in the extraliposomal media. A lower concentration (25 mM; approx. 0.94%, w/w) of CF compared with those in other retention studies (e.g., 100 mM) was used for the experiment to reduce its osmotic effect on the freezing behavior of the liposomes. A thermal transition ($T_g' = -36.2$°C) and absence of other peaks in the heating process of a frozen CF solution (25 mM in Tris–HCl buffer, pH 7.4) indicated that the solute was in a noncrystalline state in the freeze-concentrated phase. The CF-loaded liposome suspensions showed small intraliposomal solution freezing exotherms essentially identical to those of the marker-free samples in the absence of trehalose (Figs. 2 and 9). The liposomes lost a large fraction of the markers upon freeze–thawing of the trehalose-free suspensions cooled down to −35°C (below bulk solution freezing temperature) and −70°C (below intraliposomal solution freezing temperature) at all speeds (Fig. 10).

The DPPC liposomes containing trehalose on both sides of the membrane retained higher intraliposomal solution and encapsulated CF contents under faster cooling (5 and 10°C/min). Small changes of the marker retention in the fast cooling of the suspensions down to −35°C and −70°C suggested that the intraliposomal freezing by itself is not a main cause of the severe marker leakage, at least in the presence of trehalose. A large loss of the intraliposomal solution and

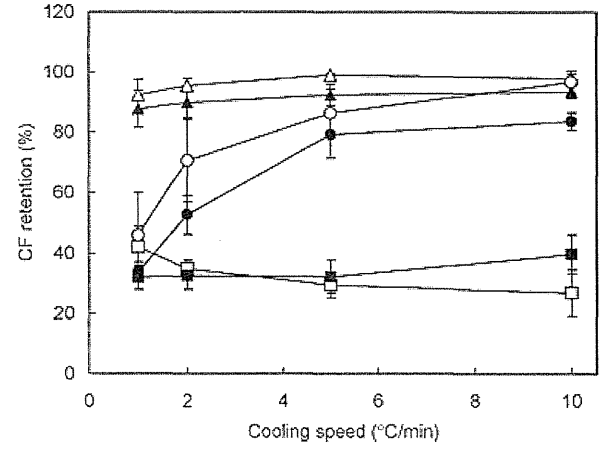

Figure 10. Effect of freeze–thawing on retention of carboxyfluorescein (CF) encapsulated in DPPC liposomes. Aliquots of CF (25 mM)-containing DPPC liposome suspension (10 μL, 4% lipid in 10 mM Tris–HCl buffer, 0.2 μm) without (□, ■) or with 12% trehalose on the outside (△, ▲) or both sides (○, ●) of the liposome membrane were cooled from room temperature to −35°C (open symbols) or −70°C (closed symbols) at 1–10°C/min, and then heated at 10°C/min (average ± SD, $n = 3$).

an accompanying apparent leakage of the marker in the slowly cooled suspensions suggested that membrane damage had occurred that allowed outbound flow of the marker-containing solution during the freezing process. Experiencing the fast-dehydrating temperature range twice in a freeze–thawing cycle should explain the larger change in marker retention compared with that of the intraliposomal freezing exotherm obtained in some cooling procedures. Suspensions containing CF and trehalose only in the intraliposomal solution also showed large intraliposomal solution freezing exotherms (Figs. 4a and 9). Solidification of the suspensions upon freeze–thawing, which hindered the CF retention measurement, confirmed the requirement of trehalose in the extraliposomal media (data not shown).[16]

The externally added trehalose (12%) reduced the CF leakage from the DPPC liposomes upon freeze–thawing at all cooling speeds. The suspensions showed a minor exotherm during the intraliposomal solution freezing. Possible osmotic shrinkage prior to freezing is the likely explanation for the limited internal solution content and the high retention of the encapsulated marker.[4,22,26] The addition of trehalose to the extraliposomal media (12%) induced leakage of less than 1% of the encapsulated CF at room temperature (data not shown).[40] Changes in the color of CF-containing liposome suspensions from yellow to orange by the extraliposomal trehalose suggested an increasing intraliposomal marker concentration due to outbound water flow through membrane diffusion (osmotic shrinkage). The lower intraliposomal solution contents should lead to the limited freeze-induced dehydration and membrane damage. The extraliposomal saccharides should also protect liposomes from membrane injury due to the growing ice surface, an excess concentration of unfavorable solutes (e.g., inorganic salts), and direct contact of concentrated liposome membranes as spacer.[40,39]

Liposome Stabilization by Control of the Osmotic Flow and Internal Freezing

The results indicated varied effect of trehalose on the freezing behavior and functional stability of liposomes upon freeze–thawing depending on its distribution across the membrane. A schematic flow of the liposome freezing behavior is shown in Figure 11. Understanding the physical changes and the encountering stresses should be relevant for strategic stabilization in freeze–thawing and freeze-drying of liposomes. Liposomes prepared by extrusion often do not contain sufficient solutions to fill the spherical structure.[37,41] Exposure of the liposomes either increases (e.g., osmotic swelling in hypotonic media) or decreases (e.g., osmotic shrinkage in hypertonic media) the internal solution content via water diffusion through the membranes. The bulk and intraliposomal solutions freeze at different temperatures, as the processes are initiated by the heterogeneous and homogeneous ice nucleation mechanisms, respectively. The freeze-induced osmotic dehydration and the intraliposomal solution freezing initiated by membrane-penetrating ice crystals should reduce intraliposomal solution content that freeze at the homogeneous ice nucleation temperature.[12,16,34,42] Accordingly, the intraliposomal solution should be in the dehydrated, supercooled, or frozen states in the frozen suspensions depending on the formulation and process factors. The absence of crystallizing solutes (e.g., mannitol) allowed observation of the freeze-induced physical changes through thermal analysis.[28]

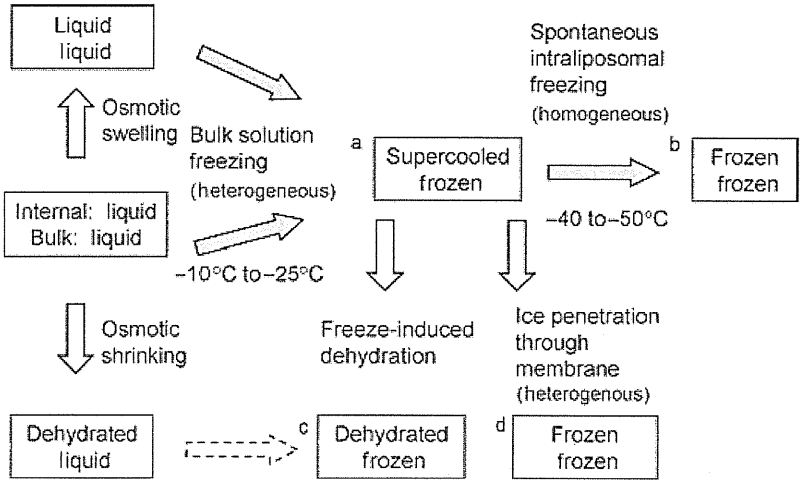

Figure 11. Schematic freezing behaviors of extruded liposome suspensions. The upper and lower rows in each box denote the physical state of the intraliposomal and bulk solutions, respectively. Boxes (a) to (d) indicate suggested physical states of frozen liposome suspensions.

DOI 10.1002/jps

Each step of the freeze-related physical changes induces stresses that affect the stability of liposomes. The growing ice during the bulk and intraliposomal solution freezing should physically damage the liposome membranes. It is possible that the freeze-induced large difference in the osmotic pressure causes larger membrane damage in the DPPC liposomes than in the living cells because of their lower hydraulic permeability, leading to a dehydrating flow of the CF-containing intraliposomal solutions. The liposomes should also experience stresses by ice crystal size growth (Ostwald ripening) and rapid dilution of the surrounding media during the thawing process of the frozen suspensions.[23,43]

The different stability-determining factors during the freezing process of the marker-loaded liposomes from those of the living cells suggest requirement of different strategies for their stabilization.[44] Trehalose protected the marker-loaded liposomes through two types of osmotic effects that prevent the freeze-induced internal solution loss during freeze–thawing. The addition of trehalose to both sides of the liposome membrane prevented both the freeze-induced dehydration and water-soluble marker loss, particularly in the higher cooling rate. The marker retention was also achieved by extraliposomal trehalose that osmotically dehydrates the liposomes through outbound water diffusion without apparent CF release in the initial suspensions. The prior dehydration should prevent the freeze-induced membrane damage even in the slower cooling. These osmotic effects should contribute as one of the major mechanisms by which trehalose protects liposomes during the freezing process besides the water-substitution, bulking, and molecular mobility reduction. The liposomes containing sufficiently high concentrations of cryoprotectants can be vitrified without the apparent ice formation by ultrafast cooling (e.g., immersion of small volume suspensions in liquid nitrogen). The vitrification method would not be practical for large-scale freezing of liposome formulations, although it is a popular way to avoid intracellular freezing during cryopreservation of living cells.[12] Formulation and process optimization of liposome pharmaceuticals should be performed through multiple assay methods (e.g., API retention, liposome fusion, aggregation, and activity of encapsulated enzyme) that appropriately detect the changes caused by different stresses.

The varied physical states of the intraliposomal solutions in the frozen suspensions should directly (e.g., membrane damage due to ice growth) or indirectly (e.g., altered excipient–membrane interactions) affect the liposome stability during freeze-drying process and subsequent storage.[1,5,8,45] The trehalose molecules are required to be distributed in the position spatially accessible to the membrane phospholipids to form the water-substituting interactions that protect the membrane structure from the dehydration stresses. The higher glass transition temperatures (T_g) of the dried solids and resistance against changes by absorbed water should make trehalose a potent stabilizer for lyophilization and subsequent storage of liposomes and biomacromolecules.[39] How the altered freezing behavior affects liposome stability during freeze-drying is an intriguing topic for further study.

The present results indicate the relevance of characterizing the freeze-related physical changes of liposomes for the development of frozen or freeze-dried formulations. The liposome composition and trehalose distribution across the membrane significantly affected the osmotic solution flows that determine the physical states of their intraliposomal solutions and functional stabilities (e.g., CF retention) upon freeze–thawing. Potentially varied molecular interactions between components would also affect liposome stability in the subsequent drying process and in storage. Controlling the osmotically mediated physical changes through formulation design and process optimization would be valuable in the cryopreservation and freeze-drying of liposome pharmaceuticals.

REFERENCES

1. Chen C, Han D, Cai C, Tang X. 2010. An overview of liposome lyophilization and its future potential. J Control Release 142:299–311.
2. Misra A, Jinturkar K, Patel D, Lalani J, Chougule M. 2009. Recent advances in liposomal dry powder formulations: Preparation and evaluation. Expert Opin Drug Deliv 6:71–89.
3. van Winden EC. 2003. Freeze-drying of liposomes: Theory and practice. Methods Enzymol 367:99–110.
4. Wessman P, Edwards K, Mahlin D. 2010. Structural effects caused by spray- and freeze-drying of liposomes and bilayer disks. J Pharm Sci 99:2032–2048.
5. Nakagaki M, Nagase H, Ueda H. 1992. Stabilization of the lamellar structure of phosphatidylcholine by complex formation with trehalose. J Memb Sci 73:173–180.
6. Crowe JH, Crowe LM, Chapman D. 1984. Preservation of membranes in anhydrobiotic organisms: The role of trehalose. Science 223:701–703.
7. Ausborn M, Schreierb H, Brezesinskic G, Fabiand H, Meyere HW, Nuhna P. 1994. The protective effect of free and membrane-bound cryoprotectants during freezing and freeze-drying of liposomes. J Control Release 30:105–116.
8. Crowe JH, Crowe LM, Carpenter JF, Rudolph AS, Wistrom CA, Spargo BJ, Anchordoguy TJ. 1988. Interactions of sugars with membranes. Biochim Biophys Acta 947:367–384.
9. Wolfe J, Bryant G. 1999. Freezing, drying, and/or vitrification of membrane-solute-water systems. Cryobiology 39:103–129.
10. Lovelock JE. 1954. The protective action of neutral solutes against haemolysis by freezing and thawing. Biochem J 56:265–270.
11. Rasmussen DH, Macaulay MN, MacKenzie AP. 1975. Supercooling and nucleation of ice in single cells. Cryobiology 12:328–339.
12. Mazur P. 1984. Freezing of living cells: Mechanisms and implications. Am J Physiol 247:C125–C142.

13. Shirakashi R, Tanasawa I. 1998. Method of designing prefreezing protocol in cryopreservation of biological materials. Ann N Y Acad Sci 858:175–182.
14. Mathias SF, Franks F, Hatley RH. 1985. Preservation of viable cells in the undercooled state. Cryobiology 22:537–546.
15. Siow LF, Rades T, Lim MH. 2007. Characterizing the freezing behavior of liposomes as a tool to understand the cryopreservation procedures. Cryobiology 55:210–221.
16. Siow LF, Rades T, Lim MH. 2008. Cryo-responses of two types of large unilamellar vesicles in the presence of non-permeable or permeable cryoprotecting agents. Cryobiology 57:276–285.
17. Talsma H, Van Steenbergen MJ, Crommelin DJ. 1992. The cryopreservation of liposomes. 2. Effect of particle size on crystallization behavior and marker retention. Cryobiology 29:80–86.
18. Charoenrein S, Reid DS. 1989. The use of DSC to study the kinetics of heterogeneous and homogeneous nucleation of ice in aqueous systems. Thermochim Acta 156:373–381.
19. Seki S, Kleinhans FW, Mazur P. 2009. Intracellular ice formation in yeast cells vs. cooling rate: Predictions from modeling vs. experimental observations by differential scanning calorimetry. Cryobiology 58:157–165.
20. Bronshteyn VL, Steponkus PL. 1993. Calorimetric studies of freeze-induced dehydration of phospholipids. Biophys J 65:1853–1865.
21. Lefevre T, Toscani S, Picquart M, Dugue J. 2002. Crystallization of water in multilamellar vesicles. Eur Biophys J 31:126–135.
22. Siminovitch D, Chapman D. 1971. Liposome bilayer model systems of freezing living cells. FEBS Lett 16:207–212.
23. Talsma H, Steenbergen MJV, Crommelin DJA. 1991. The cryopreservation of liposomes: 3. Almost complete retention of a water-soluble marker in small liposomes in a cryoprotectant containing dispersion after a freezing/thawing cycle. Int J Pharm 77:119–126.
24. Harrigan PR, Madden TD, Cullis PR. 1990. Protection of liposomes during dehydration or freezing. Chem Phys Lipids 52:139–149.
25. Higgins J, Hodges NA, Olliff CJ, Phillips AJ. 1986. Factors influencing cryoprotective activity and drug leakage from liposomes after freezing. J Pharm Pharmacol 38:259–263.
26. Hupfeld S, Moen HH, Ausbacher D, Haas H, Brandl M. 2010. Liposome fractionation and size analysis by asymmetrical flow field-flow fractionation/multi-angle light scattering: Influence of ionic strength and osmotic pressure of the carrier liquid. Chem Phys Lipids 163:141–147.
27. Ohtake S, Schebor C, Palecek SP, de Pablo JJ. 2005. Phase behavior of freeze-dried phospholipid-cholesterol mixtures stabilized with trehalose. Biochim Biophys Acta 1713:57–64.
28. Talsma H, van Steenbergen MJ, Salemink PJ, Crommelin DJ. 1991. The cryopreservation of liposomes. 1. A differential scanning calorimetry study of the thermal behavior of a liposome dispersion containing mannitol during freezing/thawing. Pharm Res 8:1021–1026.
29. MacDonald RC, MacDonald RI, Menco BP, Takeshita K, Subbarao NK, Hu LR. 1991. Small-volume extrusion apparatus for preparation of large, unilamellar vesicles. Biochim Biophys Acta 1061:297–303.
30. Kristiansen J. 1992. Leakage of a trapped fluorescent marker from liposomes: Effects of eutectic crystallization of NaCl and internal freezing. Cryobiology 29:575–584.
31. Bartlett GR. 1959. Phosphorus assay in column chromatography. J Biol Chem 234:466–468.
32. Kaasgaard T, Mouritsen OG, Jørgensen K. 2003. Freeze/thaw effects on lipid-bilayer vesicles investigated by differential scanning calorimetry. Biochim Biophys Acta 1615:77–83.
33. Wu WG, Chi LM, Yang TS, Fang SY. 1991. Freezing of phosphocholine headgroup in fully hydrated sphingomyelin bilayers and its effect on the dynamics of nonfreezable water at subzero temperatures. J Biol Chem 266:13602–13606.
34. Rall WF, Mazur P, McGrath JJ. 1983. Depression of the ice-nucleation temperature of rapidly cooled mouse embryos by glycerol and dimethyl sulfoxide. Biophys J 41:1–12.
35. Nagle JF, Wilkinson DA. 1978. Lecithin bilayers. Density measurement and molecular interactions. Biophys J 23:159–319.
36. Koster KL, Lei YP, Anderson M, Martin S, Bryant G. 2000. Effects of vitrified and nonvitrified sugars on phosphatidylcholine fluid-to-gel phase transitions. Biophys J 78:1932–1946.
37. Mui BL, Cullis PR, Evans EA, Madden TD. 1993. Osmotic properties of large unilamellar vesicles prepared by extrusion. Biophys J 64:443–453.
38. Akers MJ, Vasudevan V, Stickelmeyer M. 2002. Formulation development of protein dosage forms. Pharm Biotechnol 14:47–127.
39. Nail SL, Jiang S, Chongprasert S, Knopp SA. 2002. Fundamentals of freeze-drying. Pharm Biotechnol 14:281–360.
40. Blok MC, van Deenen LL, De Gier J. 1976. Effect of the gel to liquid crystalline phase transition on the osmotic behaviour of phosphatidylcholine liposomes. Biochim Biophys Acta 433:1–12.
41. Pencer J, White GF, Hallett FR. 2001. Osmotically induced shape changes of large unilamellar vesicles measured by dynamic light scattering. Biophys J 81:2716–2728.
42. Suzuki T, Komatsu H, Miyajima K. 1996. Effects of glucose and its oligomers on the stability of freeze-dried liposomes. Biochim Biophys Acta 1278:176–182.
43. Grabielle-Madelmont C, Perron R. 1983. Calorimetric studies on phospholipid-water systems: II. Study of water behavior. J Colloid Interface Sci 95:483–493.
44. Hubel A, Darr TB, Chang A, Dantzig J. 2007. Cell partitioning during the directional solidification of trehalose solutions. Cryobiology 55:182–188.
45. Ohtake S, Schebor C, de Pablo JJ. 2006. Effects of trehalose on the phase behavior of DPPC-cholesterol unilamellar vesicles. Biochim Biophys Acta 1758:65–73.

Feasibility of Atomic Force Microscopy for Determining Crystal Growth Rates of Nifedipine at the Surface of Amorphous Solids with and Without Polymers

TAMAKI MIYAZAKI, YUKIO ASO, TORU KAWANISHI

Division of Drugs, National Institute of Health Sciences, Setagaya-ku, Tokyo 158-8501, Japan

Received 21 February 2011; revised 31 March 2011; accepted 18 April 2011

Published online 3 May 2011 in Wiley Online Library (wileyonlinelibrary.com). DOI 10.1002/jps.22603

ABSTRACT: Amorphous nifedipine (NFD), which has a smooth surface immediately after preparation, was shown to have structures resembling clusters of curling and branching fibers approximately 1 μm wide by atomic force microscopy (AFM) after storage at 25°C. The size of the cluster-like structures increased with storage over time, implying crystal growth. The average elongation rate of the fibers determined by AFM at ambient room temperature was 1.1×10^{-9} m/s, and this agreed well with the crystal growth rate of 1.6×10^{-9} m/s determined by polarized light microscopy. The crystal growth rate of NFD in solid dispersions with 5% polyethylene glycol (PEG) was found to be 5.0×10^{-8} m/s by AFM. Although this value was approximately the same as that obtained by polarized light microscopy, three-dimensional information obtained by AFM for the crystallization of NFD in a solid dispersion with PEG revealed that the changes in topography were not a consequence of surface crystal growth, but rather attributable to the growth of crystals formed in the amorphous bulk. For solid dispersions with α,β-poly(N-5-hydroxypentyl)-L-aspartamide, acceleration of NFD crystallization by tapping with an AFM probe was observed. The present study has demonstrated the feasibility and application of AFM for interpretation of surface crystallization data. © 2011 Wiley-Liss, Inc. and the American Pharmacists Association J Pharm Sci 100:4413–4420, 2011

Keywords: amorphous; crystallization; excipients; physical stability; solid dispersion; microscopy

INTRODUCTION

Amorphous drugs are generally more soluble and dissolve faster than their crystalline counterparts.[1–3] Therefore, amorphization of poorly water-soluble drugs is a useful method for enhancing their dissolution rate and consequently improving their bioavailability. However, the amorphous form is thermodynamically unstable and tends to revert to its crystalline form, resulting in loss of the solubility advantage. Recently, surface-enhanced crystallization of indomethacin[4] and nifedipine (NFD)[5] has been reported. The crystal growth rates of amorphous indomethacin and NFD at the free surface were orders of magnitude faster than those in bulk at temperatures below their glass transition temperature (T_g). Microscopic observation of partially crystallized indomethacin and NFD samples has revealed that crystallized drugs are localized at the surface of the samples.[5] Once the surface is covered with a crystal layer, the solubility advantage is lost even if the most interior part of the solid remains amorphous.

Atomic force microscopy (AFM), which can capture surface topography images of solid samples with a resolution of the micrometer order or less, may be a useful tool for investigating the surface crystallization of pharmaceuticals. The crystallization of cholesterol under conditions simulating the gallbladder environment has been studied by AFM.[6] Cholesterol crystals of submicrometer size have been observed on the surface of mica and mucin-coated mica, but no such crystals have been found on the surface of silanized mica, suggesting that a network of hydrogen bonds on the surface provides favorable conditions for the nucleation and growth of cholesterol crystals. Molecular rearrangements at the surface have been observed for caffeine/carboxylic acid cocrystals by AFM.[7] The depth and width of trenches aligned

Correspondence to: Tamaki Miyazaki (Telephone: +81-3-3700-1141; Fax: +81-3-3707-6950; E-mail: miyazaki@nihs.go.jp)

Journal of Pharmaceutical Sciences, Vol. 100, 4413–4420 (2011)
© 2011 Wiley-Liss, Inc. and the American Pharmacists Association

along the needle-shaped crystal axis have been shown to increase during storage for 2–7 days under dry and humid conditions, and regular triangular or rectangular features have been observed, indicating surface recrystallization of caffeine cocrystals. Changes in the surface topology of spray-dried lactose particles have also been observed by AFM.[8] Linear striated features due to crystallization appeared and gradually propagated across the surface of the particles stored at 58% relative humidity. The crystallized surface had an irregular topology with a well-ordered and definable structure over relatively small areas but not over wide areas, suggesting that secondary nucleation and growth had occurred. Furthermore, the surface crystallization rate of spray-dried amorphous lactose has been reported.[9,10] Images of rectangular shapes on the surface of the lactose particles have been sequentially captured as a function of time by AFM, and the growth rate has been estimated from the time profiles of width and length of the rectangular shapes.

The aim of this study was to investigate the feasibility of AFM for determining crystal growth rates at the surface of amorphous NFD in the presence and absence of polymer excipients by capturing sequential images in specific areas of the samples. The polymer excipients used were polyethylene glycol (PEG) and α,β-poly(N-5-hydroxypentyl)-L-aspartamide (PHPA). PEG is one of the typical polymers used for preparation of solid dispersions to improve drug dissolution.[11–13] PHPA has been selected as a model of a partially immiscible polymer with NFD[14] because the miscibility of an amorphous drug with polymer excipients is one of the factors that determine the physical stability of amorphous solid dispersions.[15] Here, we compared the growth rates estimated from AFM measurements with the values estimated from polarized light microscopy measurements. Spatial information on the crystallization of NFD alone and that in these solid dispersions obtained by AFM is described.

EXPERIMENTAL

Materials and Sample Preparation

Nifedipine was obtained from Sigma–Aldrich Company (St. Louis, MO). PEG with an average molecular weight of 300 was purchased from Wako Pure Chemical Industries Ltd. (Osaka, Japan). PHPA was synthesized via polycondensation of L-aspartic acid and 1-aminopentane using a method similar to that reported previously.[16]

The sample of amorphous NFD was prepared on a glass plate as follows: Crystalline NFD (approximately 20 mg) was put on a glass plate (thickness 0.12–0.17 mm, diameter 18 mm), and the plate was placed in a differential scanning calorimeter (DSC2920; TA Instruments, New Castle, DE) at 190°C for approximately 2 min under dry nitrogen flow (30 mL/min). Then, the glass plate was removed from the differential scanning calorimeter and cooled to room temperature on a stainless steel block for several seconds. The samples were stored in a desiccator over phosphorous pentoxide to avoid moisture, and were kept at 25°C before AFM measurements. Amorphous NFD samples containing PEG or PHPA were prepared as described above using approximately 20 mg of NFD–polymer mixtures, which were obtained by solvent evaporation of NFD–PEG methanol solution and NFD–PHPA ethanol solution.

Amorphous NFD containing PEG was also prepared in a glass Petri dish (inner diameter 23 mm, depth 7 mm) to visually examine positions of NFD crystallization in the NFD–PEG solid dispersion. Approximately 2 g of NFD–PEG (5%) mixture in the Petri dish was kept at 197°C for 5 min in an oven, and then quenched on a stainless steel block that had been precooled with ice.

AFM Measurements

Atomic force microscopy (Dimension 3100; Veeco Instruments, Plainview, NY) measurements were performed in tapping mode, analogous to noncontact mode and alternating current mode, under ambient temperature (26±1°C) and relative humidity (<50%). The operation software used was Nanoscope 5.30r1 (Veeco Instruments). Silicon probes with a nominal spring constant of 42 N/m and a nominal length of 125 μm were used. AFM images were collected at a scan speed of 50–150 μm/s for a square region of 50–100 μm with 256–512 collecting points per line. The topography images were collected by scanning the probe across the surface of the sample in a raster pattern, line by line, from one side of the square area toward the opposing side. Because the scan direction changed alternately from downward and upward during sequential data collection, only the images collected in the downward scan direction were used to determine the crystal growth rate. To investigate the potential effects of physical stimulation from the AFM probe on the crystal growth rate of NFD, AFM images were collected at various time intervals (1.3–17 min/image) by varying the scan range, scan speed, and collecting points per line.

Measurements of Crystal Growth Rate by Polarized Light Microscopy

Crystal growth rates of NFD in amorphous NFD alone and NFD–polymer solid dispersions were determined using a polarized light microscope (ECLIPSE E600 POL; Nikon Corporation, Tokyo, Japan) with a ×10 objective lens (depth of field 8.46 μm). The microscope was equipped with a heating/cooling

 DOI 10.1002/jps

stage (THMS600; Linkam Scientific Instruments, Tadworth, Surrey, UK) to control the temperature of the sample. The sample of amorphous NFD, prepared as described above, was placed in the chamber of the heating/cooling stage, which had been preheated to 25°C. Then, the chamber was purged with dry nitrogen gas for 5–10 min to remove moisture, and hermetically closed. The focus of the microscope was adjusted to the free surface of the amorphous sample, and the crystal growth was observed. Microscopy images were recorded at constant time intervals by a digital camera (DXM1200F; Nikon Corporation) attached to the microscope, and were analyzed using Lumina Vision software (Mitani Company, Fukui, Japan). The crystal growth rates were estimated from the increase in size of the crystals with storage time.

Differential Scanning Calorimetry Measurements

Glass transition temperature values of the amorphous NFD and NFD–polymer solid dispersions were determined by differential scanning calorimetry (DSC) measurement. Indium was used to calibrate the cell constant and the temperature of the instrument. The DSC cell was purged constantly by dry nitrogen gas flow at 30 mL/min. Crystalline NFD or NFD–polymer mixed powder (approximately 5 mg) in a hermetic aluminum pan was heated to 190°C at a heating rate of 20°C/min, kept at that temperature for 90 s, and then cooled to −80°C at a cooling rate of 40°C/min by pouring liquid nitrogen into a cooling jacket surrounding the DSC cell. The T_g was obtained on the second heating run at a rate of 20°C/min.

The melting point of recrystallized NFD was measured by DSC. After AFM observation, the sample was stored in a desiccator over phosphorous pentoxide at 25°C to complete the recrystallization. Completion of the recrystallization took approximately 3 months for pure NFD, 1 month for NFD–PEG solid dispersions, and a $\frac{1}{2}$ year for NFD–PHPA solid dispersions. The recrystallized sample (5–10 mg) was scratched off from the glass plate into a hermetic aluminum pan, and the melting point of the sample was measured at a heating rate of 20°C/min.

RESULTS AND DISCUSSION

Amorphous NFD Without Polymer

Figure 1 shows typical AFM images of amorphous NFD. Amorphous NFD exhibited a smooth surface immediately after preparation as shown in Figure 1a. The root-mean-square value of the surface roughness was less than 0.5 nm for freshly prepared amorphous samples. After storage at 25°C, structures resembling clusters of curling and branching fibers with a width of approximately 1 μm appeared on the surface as shown in Figure 1b. The size of these structures increased with storage time, suggesting that they were NFD crystals that had formed during storage. The height of the crystals was approximately 1 μm, and hardly this changed even when the scanning area for AFM was covered by NFD crystals. This suggested that NFD crystals preferentially grew along the surface than toward the inner part of the sample. This speculation is supported by the fact that the inner part of the NFD sample after AFM measurements was transparent, indicating that the interior of the samples remained amorphous even after the surface had crystallized. Faster crystal growth of NFD at the surface of amorphous solids has been reported by Zhu et al.[5] They found that the crystal growth of NFD occurred preferentially at the free surface of the amorphous sample when it was exposed to air by removing one glass plate from a sample that had been prepared between two glass plates. The crystal shape reported by Zhu et al.[5] was similar to that shown in Figure 1b.

The crystal form of NFD observed by AFM was determined from the melting point of the recrystallized samples. Figure 2 shows DSC thermograms of crystalline NFD and completely recrystallized NFD, which had been stored as amorphous NFD at 25°C for approximately 3 months after AFM measurements. The recrystallized NFD showed an endothermic peak at approximately 171°C (Fig. 2b), suggesting that a stable form of NFD crystal (Fig. 2a) is formed during storage at 25°C.

Serial AFM images of partially recrystallized amorphous NFD were captured continuously in the same area to determine the crystal growth rate of NFD at

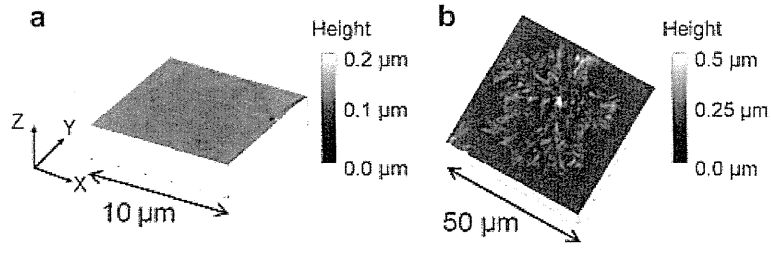

Figure 1. Representative atomic force microscopy images of amorphous nifedipine (a) immediately after preparation and (b) after storage at 25°C.

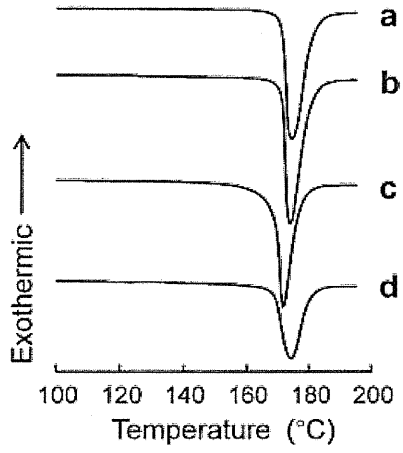

Figure 2. Differential scanning calorimeter thermograms for (a) nifedipine (NFD) in stable form, NFD recrystallized at 25°C from amorphous (b) NFD without polymer, (c) NFD–polyethylene glycol (5%) solid dispersion, and (d) NFD–α,β-poly(N-5-hydroxypentyl)-L-aspartamide (30%) solid dispersion.

the surface. Figure 3 shows typical images representing crystal growth of NFD at the surface. The time required to capture one image was approximately 17 min for this series of measurements. Using image analysis software, the crystal growth rate was determined from the coordinates (x_A, y_A) and (x_B, y_B), which are the end points of one crystal indicated by A in the image after 68 min and B in the image after 102 min, respectively. The growth rate was calculated by dividing the distance between (x_A, y_A) and (x_B, y_B) by the time interval, 34 min. In order to confirm that the physical stimulation from the AFM probe did not affect the crystal growth rate of NFD, AFM images were collected at various time intervals by varying the experimental conditions (scan range, scan speed, and collecting points per line). If the physical stimulus of tapping affected the crystal growth, the estimated growth rates have differed depending on the interval employed for image collection. Growth rates estimated under various experimental conditions are shown in Table 1. Because differences in the estimated growth rates lay within experimental error range regardless of the interval used for image collection, any influence of tapping by the AFM probe on the crystal growth rate was considered to be negligible. The NFD crystal growth rate was also estimated by polarized light microscopy using some pairs of micrographs recorded when the microscope was focused on the surface of the amorphous solid (Table 1). The crystal growth rates of NFD determined from the data obtained by AFM and polarized light microscopy agreed well, and the growth rates determined in the present study were similar to those reported by Zhu et al.[5] for the crystal growth rate at the free surface of amorphous NFD solids.

NFD Solid Dispersions with PEG

The surface of NFD solid dispersions containing PEG was smooth immediately after preparation (images not shown). Figure 4 shows representative AFM images after storage at 25°C for approximately 1 day. NFD–PEG (5%) solid dispersions exhibited dimples at the surface, as shown in Figure 4a. Dimples with a depth of more than 5.7 μm (the operational limit of the AFM probe) were sometimes observed. After longer storage, spiky structures were observed in the dimples, as shown in Figure 4b, and the area with an apparently rough surface increased with time. Crystals were detected by polarized light microscopy in the positions where the dimples, with and without spiky structures, had been observed by AFM. This implies that the formation of dimples and spiky structures is associated with NFD crystallization during storage. Figure 5 shows a partially crystallized NFD–PEG (5%) solid dispersion prepared in a small glass Petri dish. After storage at 25°C for approximately 15 h, some crystals grew at the surface, as circled by dotted lines (Fig. 5a), although most of them were observed randomly in the bulk (Figs. 5a and 5b). These results indicated that NFD crystallization was not always initiated at the surface of NFD–PEG solid dispersions. The dimples at the surface observed by AFM may have been formed by volume reduction upon crystallization of amorphous NFD initiated in the bulk, but not so far from the sample surface. Therefore, it may take some time for the crystals with spiky structures to become apparent at the sample surface, as shown in Figure 4b. These results suggest that AFM measurements discriminate the position where crystallization has initiated (at the surface or in the bulk), and the

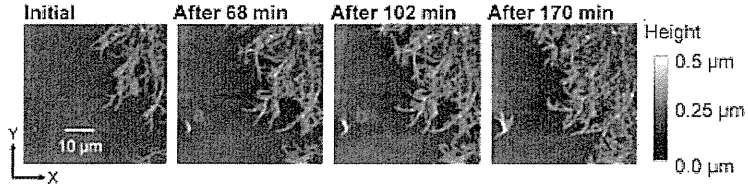

Figure 3. Serial atomic force microscopy images representing crystal growth at the surface of amorphous nifedipine without polymer at ambient temperature (26 ± 1°C).

DOI 10.1002/jps

Table 1. T_g Values Determined by DSC, and NFD Crystal Growth Rates Obtained by AFM and Polarized Light Microscopy at Around 25°C

		AFM Experimental Conditions				Crystal Growth Rate (m/s)	
	T_g (°C)	Scan Range (μm)	Scan Speed (μm/s)	Collected Points Per Line	Collection Interval[a] (min)	AFM	Polarized Light Microscopy
NFD	46.2 ± 0.5[b]	100	75	256	5.3	(1.2 ± 0.3) × 10^{-9}[c]	(1.6 ± 0.4) × 10^{-9}[d]
		100	50	256	8.6	(1.1 ± 0.3) × 10^{-9}[c]	
		50	50	512	8.6	(1.0 ± 0.2) × 10^{-9}[c]	
		100	50	512	17	(1.3 ± 0.4) × 10^{-9}[c]	
NFD–PEG (5%)	33.5 ± 0.6[b]	100	150	256	2.6	5.1 × 10^{-8}	(7.2 ± 1.7) × 10^{-8}[e]
		80	150	256	2.2	6.3 × 10^{-8}	
		50	150	256	1.3	4.9 × 10^{-8}	
		100	100	256	4.3	4.5 × 10^{-8}	

[a]Time required to collect one image.
[b]Average with standard deviation ($n = 5$).
[c]Average with standard deviation ($n > 9$ points for each five samples).
[d]Average with standard deviation ($n > 5$ points for each five samples).
[e]Average with standard deviation ($n = 6$).
AFM, atomic force microscopy; NFD, nifedipine; PEG, polyethylene glycol.

direction of crystal growth (along the surface or into the bulk): characteristics that are difficult to determine by polarized light microscopy. It should be noted that even though AFM images suggest that crystals grow at the surface of samples, crystallization is not always initiated at the surface.

Although the crystal growth rate of NFD in a solid dispersion with PEG determined by AFM is not the surface growth rate, as described above, the apparent rate was estimated and compared with that obtained by polarized light microscopy. From serial AFM images exemplified by Figure 4b, the crystal growth rate of NFD in solid dispersions containing 5% PEG was determined. Because of possible changes in the NFD crystallization rate by the physical stimulus of tapping, the increase in diameter of the recrystallized domains was measured at various time intervals by varying the experimental scan range (50–100 μm) and scan speed (100–150 μm/s). Figure 6 shows the time profiles of the diameter of the recrystallized domains measured under various experimental conditions: hollow triangles and hollow squares represent the results of measurements using the shortest and the longest time intervals, respectively. The variation in slope appeared to lie within the range of experimental error, and no clear dependence of the growth rate on the time interval for collection was evident. From these results, it is considered that the influence of tapping by the AFM probe on the crystal growth rate is negligible in NFD–PEG solid dispersions. Each growth rate calculated from the slope of the plots shown in Figure 6 is listed in Table 1. The value was of the same order as that obtained by polarized light microscopy at 25°C (Table 1). The crystal growth rate of NFD in the NFD–PEG (5%) solid dispersions was approximately 50 times higher than that in amorphous NFD alone. The T_g value of the NFD–PEG (5%) solid dispersion was approximately 13° lower than that of NFD alone (Table 1), indicating that the matrix mobility of NFD–PEG is higher than that of NFD alone.

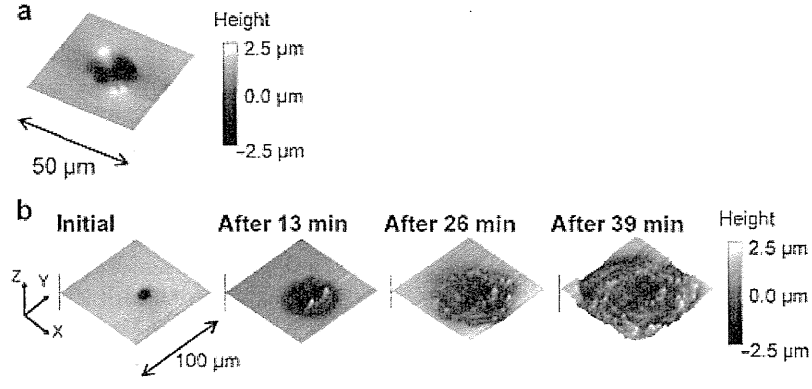

Figure 4. Atomic force microscopy images of nifedipine (NFD)–polyethylene glycol (5%) solid dispersion. (a) Partially recrystallized solid dispersion after storage at 25°C and (b) serial images representing NFD crystal growth at ambient temperature, 26 ± 1°C.

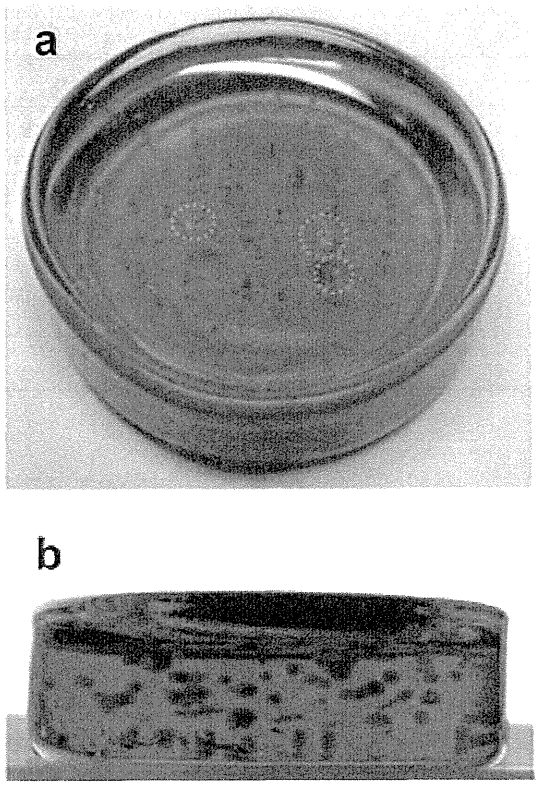

Figure 5. Partially crystallized nifedipine (NFD)–polyethylene glycol (5%) solid dispersion prepared in a small glass Petri dish (inner diameter 23 mm). The sample was stored at 25 C for approximately 15 h. Dotted green circles in the photograph (a) indicate sites of crystallization at the surface. Other dark granular shapes are NFD crystals formed in the amorphous bulk. (a) Photograph taken from top and (b) photograph taken from the side.

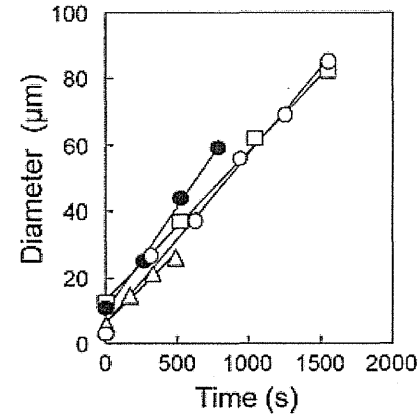

Figure 6. Increase in diameter of crystallized domains at the surface of nifedipine–polyethylene glycol (5%) solid dispersions at ambient temperature, 26 ± 1°C. The time when the first scan had been completed was defined as "time = 0" for each sequential measurement. The measurement conditions for each symbol are as follows (scan range and scan speed): ○ (100 μm, 150 μm/s), ● (80 μm, 150 μm/s), △ (50 μm, 150 μm/s), and □ (100 μm, 100 μm/s).

The increased molecular mobility of the amorphous matrix may be one of the reasons for the higher crystal growth rate in NFD–PEG solid dispersions. Another possible reason for the higher crystal growth rate may be due to the difference in the crystalline form formed in pure NFD and NFD–PEG solid dispersions during AFM measurements. Although the melting point of the recrystallized NFD in the solid dispersions containing PEG [169°C (Fig. 2c)] suggests that a stable form of NFD crystal is formed during the storage for 1 month, this result may not exclude the possibility that crystals other than stable form have been formed in the solid dispersions during AFM measurements.

NFD Solid Dispersions with PHPA

Figure 7a shows a typical AFM image of partially recrystallized NFD–PHPA solid dispersions stored at 25°C for a few weeks. The diameter and height of the cone-shaped structures increased with storage time. The melting point of the recrystallized NFD–PHPA (30%) samples stored at 25°C for approximately 6 months (169°C as shown in Fig. 2d) suggests that the crystal with a cone-shaped structure is the stable form of NFD.

Only the cone-shaped structures were observed in the first scan (Fig. 7a), but string-like structures were also observed in the image of the second scan (Fig. 7b). The area covered by the string-like structures increased gradually with each scan, as shown in Figure 7c, which is the image collected after continuous scanning for 34 min. Visual inspection of the area where AFM images were collected revealed loss of transparency in the area, suggesting crystallization of NFD. During the measurements, the size of the originally existing cone-shaped structures did not change (images not shown). Figure 7d shows an image of a different site in the same sample, wherein the AFM probe had not made contact, obtained after scanning the image shown in Figure 7c. No string-like structures were evident. These results suggest that physical stimulation by tapping with the AFM probe caused acceleration of new NFD crystal formation and growth at the surface of solid dispersions containing 30% PHPA. This acceleration effect was also observed for solid dispersions containing up to 70% PHPA. The reason why tapping by the AFM probe only accelerates the formation and growth of string-like crystals is still unclear. NFD is partially immiscible with PHPA. The presence of at least two different phases in the solid dispersion was indicated by the biexponential decay patterns of ^{1}H NMR spin-lattice relaxation.[14]

 DOI 10.1002/jps

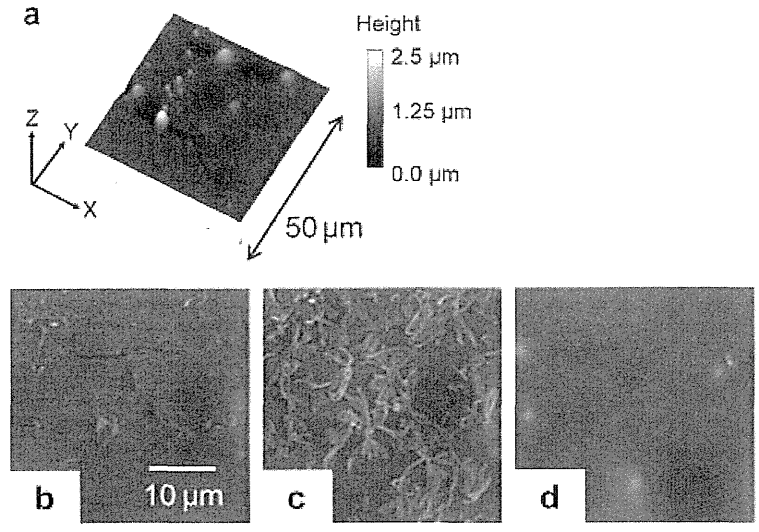

Figure 7. Atomic force microscopy images of nifedipine–α,β-poly(N-5-hydroxypentyl)-L-aspartamide (30%) solid dispersion. (a) The first scan of the partially crystallized sample stored at 25 C for over 1 month, (b) the second scan, (c) after continuous scanning for 34 min, (d) a different site in the same sample after measurement (c). The area for images (b) and (c) corresponds to approximately one-fourth of the bottom-right corner of the image (a).

The finding that the NFD–PHPA solid dispersions exhibit two T_gs has also supported the partial immiscibility between NFD and PHPA.[14] T_gs at 46°C and 70°C for the NFD–PHPA (30%) solid dispersions may correspond to the T_g of amorphous NFD alone and that of the NFD–PHPA matrix, respectively. NFD may be present in a supersaturated state, and may be more sensitive to the physical stimulation of tapping than amorphous NFD without polymer or with PEG.

CONCLUSIONS

Atomic force microscopy was found to be a useful tool for studying the crystallization kinetics of amorphous solids by targeting crystals at the surface. The ability to obtain three-dimensional information at the surface is one of the advantages of AFM, as well as its nanoscale resolution, enabling it to detect minute topographical changes that can indicate the crystal growth rate in a short time. However, two phenomena revealed in this study need to be borne in mind when interpreting the data obtained by AFM measurements: (1) Although crystal structures are captured at the surface of the sample by AFM, the crystal formation may not always be initiated at the surface. The change in surface topography may reflect the growth of crystals from the bulk. (2) Physical stimulation by the AFM probe may affect the crystallization rate, as shown for NFD crystallization in NFD–PHPA solid dispersions.

ACKNOWLEDGMENTS

Part of this work was supported by a grant-in-aid for Research on Publicly Essential Drugs and Medical Devices from The Japan Health Sciences Foundation.

REFERENCES

1. Bunjes H, Rades T. 2005. Thermotropic liquid crystalline drugs. J Pharm Pharmacol 57:807–816.
2. Murdande SB, Pikal MJ, Shanker RM, Bogner RH. 2001. Solubility advantage of amorphous pharmaceuticals: I. A thermodynamic analysis. J Pharm Sci 99:1254–1264.
3. Blagden N, de Matas M, Gavan PT, York P. 2007. Crystal engineering of active pharmaceutical ingredients to improve solubility and dissolution rates. Adv Drug Deliv Rev 59:617–630.
4. Wu T, Yu L. 2006. Surface crystallization of indomethacin below T_g. Pharm Res 23:2350–2355.
5. Zhu L, Wong L, Yu L. 2008. Surface-enhanced crystallization of amorphous nifedipine. Mol Pharm 5:921–926.
6. Liao X, Wiedmann TS. 2006. Formation of cholesterol crystals at a mucin coated substrate. Pharm Res 23:2413–2416.
7. Cassidy AM, Gardner CE, Jones W. 2009. Following the surface response of caffeine cocrystals to controlled humidity storage by atomic force microscopy. Int J Pharm 379:59–66.
8. Price R, Young PM. 2004. Visualization of the crystallization of lactose from the amorphous state. J Pharm Sci 93:155–164.
9. Mahlin D, Berggren J, Alderborn G, Engström S. 2004. Moisture-induced surface crystallization of spray-dried amorphous lactose particles studied by atomic force microscopy. J Pharm Sci 93:29–37.
10. Mahlin D, Berggren J, Gelius U, Engström S, Alderborn G. 2006. The influence of PVP incorporation on moisture-induced surface crystallization of amorphous spray-dried lactose particles. Int J Pharm 321:78–85.
11. Chan KL, Kazarian SG. 2004. FTIR spectroscopic imaging of dissolution of a solid dispersion of nifedipine in poly(ethylene glycol). Mol Pharm 1:331–335.

12. Vippagunta SR, Wang Z, Hornung S, Krill SL. 2007. Factors affecting the formation of eutectic solid dispersions and their dissolution behavior. J Pharm Sci 96:294–304.
13. Bley H, Fussnegger B, Bodmeier R. 2010. Characterization and stability of solid dispersions based on PEG/polymer blends. Int J Pharm 390:165–173.
14. Aso Y, Yoshioka S, Miyazaki T, Kawanishi T, Tanaka K, Kitamura S, Takakura A, Hayashi T, Muranushi N. 2007. Miscibility of nifedipine and hydrophilic polymers as measured by ^{1}H-NMR spin-lattice relaxation. Chem Pharm Bull 55:1227–1231.
15. Rumondor AC, Marsac PJ, Stanford LA, Taylor LS. 2009. Phase behavior of poly(vinylpyrrolidone) containing amorphous solid dispersions in the presence of moisture. Mol Pharm 6:1492–1505.
16. Giammona G, Carlisi B, Plazzo S. 1987. Reaction of α,β-poly(N-hydroxyethyl)-DL-aspartamide with derivatives of carboxylic acids. J Polym Sci Polym Chem Ed 25:2813–2818.

 DOI 10.1002/jps

PHARMACEUTICAL TECHNOLOGY

Impact of Heat Treatment on the Physical Properties of Noncrystalline Multisolute Systems Concentrated in Frozen Aqueous Solutions

KEN-ICHI IZUTSU, CHIKAKO YOMOTA, TORU KAWANISHI

National Institute of Health Sciences, Setagaya, Tokyo 158-8501, Japan

Received 8 April 2011; revised 23 June 2011; accepted 24 June 2011

Published online 20 July 2011 in Wiley Online Library (wileyonlinelibrary.com). DOI 10.1002/jps.22706

ABSTRACT: The purpose of this study was to elucidate the effect of heat treatment on the miscibility of multiple concentrated solutes that mimic biopharmaceutical formulations in frozen solutions. The first heating thermal analysis of frozen solutions containing either a low-molecular-weight saccharide (e.g., sucrose, trehalose, and glucose) or a polymer (e.g., polyvinylpyrrolidone and dextran) and their mixtures from −70°C showed a single transition at glass transition temperature of maximally freeze-concentrated solution (T_g') that indicated mixing of the freeze-concentrated multiple solutes. The heat treatment of single-solute and various polymer-rich mixture frozen solutions at temperatures far above their T_g' induced additional ice crystallization that shifted the transitions upward in the following scan. Contrarily, the heat treatment of frozen disaccharide-rich solutions induced two-step heat flow changes (T_g' splitting) that suggested separation of the solutes into multiple concentrated noncrystalline phases, different in the solute compositions. The extent of the T_g' splitting depended on the heat treatment temperature and time. Two-step glass transition was observed in some sucrose and dextran mixture solids, lyophilized after the heat treatment. Increasing mobility of solute molecules during the heat treatment should allow spatial reordering of some concentrated solute mixtures into thermodynamically favorable multiple phases. © 2011 Wiley-Liss, Inc. and the American Pharmacists Association J Pharm Sci 100:5244–5253, 2011

Keywords: freezing; freeze-drying; miscibility; phase separation; stabilization; formulation; thermal analysis; calorimetry (DSC); excipients

INTRODUCTION

Freeze-drying is a popular method of formulating certain biopharmaceuticals (e.g., therapeutic proteins and vaccines) and molecular assembly drug delivery systems (e.g., liposomes) that are not sufficiently stable in aqueous solutions during storage and distribution. Formulation and process design that protect the integrity of their higher-order structure from irreversible damages caused by various stresses (e.g., low temperature and dehydration) during the process and storage is particularly important to ensure the quality of the highly potent pharmaceuticals.[1–5] The growing clinical significance of therapeutic proteins and liposomes makes their miscibility with nonreducing disaccharides (e.g., sucrose and trehalose) in frozen solutions and subsequently dried solids an intriguing topic because their thermodynamic and kinetic stabilization mechanisms, namely water-substituting direct molecular interactions and mobility-limiting embedment in glass-state solids, both require the mixing of heterogeneous molecules.[6–10]

Assessing and controlling the component miscibility in noncrystalline solid formulations, however, are often challenging. Thermal analysis and several spectroscopic methods have been applied to estimate the miscibility of ingredients in colyophilized solids and molecular dispersion solid formulations.[6,8–11] Profiles of glass transition temperatures (T_gs) indicate nonideal mixing of colyophilized disaccharides and polymers (e.g., trehalose and dextran) in some solids.[9,10] The local inhomogeneity of a disaccharide and a polymer [e.g., polyvinylpyrrolidone (PVP) and lysozyme] in amorphous freeze-dried or hot melt-extruded mixture solids has also been reported in studies using novel spectroscopic techniques [e.g., microscopic

Correspondence to: Ken-ichi Izutsu (Telephone: +81-33700-1141; Fax: +81-33707-6950; E-mail: izutsu@nihs.go.jp)

Journal of Pharmaceutical Sciences, Vol. 100, 5244–5253 (2011)

© 2011 Wiley-Liss, Inc. and the American Pharmacists Association

near-infrared (NIR) and Raman imaging, X-ray powder diffraction (XRPD) coupled with computation of pair distribution functions].[6,8,11] The broad spectrum, small domains, and difficulties in the handling of the amorphous solids, however, limit the information available using these methods.

Elucidating how each step of the freeze-drying process affects the component miscibility would be another approach to the rational development of stable formulations. The freeze-drying process consists of freezing, primary drying (ice sublimation), and secondary drying (removal of residual water) segments.[12,13] The freezing of aqueous solutions concentrates the solutes (70%–80%, w/w) into highly viscous supercooled solutions surrounding ice crystals. The increasing concentration separates certain polymer mixtures [e.g., PVP and dextran, polyethylene glycol (PEG) and dextran] or a polymer and an inorganic salt (e.g., PVP and potassium phosphate) that were originally miscible in an aqueous solution into multiple concentrated phases rich in one of the polymers through a thermodynamic mechanism that also induces aqueous two-layer systems.[14–19] Thermal analysis of frozen solutions provides glass transition temperature of maximally freeze-concentrated solutions (T_g's) that are valuable to assess miscibility of noncrystalline solutes.[20,21] Some polymers (e.g., PEG) tend to crystallize in the phase-separated freeze-concentrated solutions.[22] Many other solutes in a solution remain miscible in a highly concentrated viscous solution upon freezing.

The purpose of this study was to elucidate the effect of heat treatment (annealing) of frozen solutions on the miscibility of freeze-concentrated disaccharide and polymer mixtures. Subjecting frozen solutions to heat treatment at above their T_g' is a popular method of inducing ice crystal size growth or crystallization of certain solutes in the pharmaceutical lyophilization.[12,13,23] The increasing ice crystal size by Ostwald ripening and resulting larger pores in the dried layer allow faster water vapor transition from advancing sublimation interfaces during the primary drying. The crystallization of some low-molecular-weight active pharmaceutical ingredients (APIs) and excipients (e.g., antibiotics and bulking agents) in the frozen solutions results in better chemical stability of the dried formulations.[24] The faster ice sublimation should also be an apparent advantage for the efficient freeze-drying of biopharmaceutical and drug delivery system (DDS) formulations; however, the application of the heat treatment to the freeze-drying of structurally and compositionally complex systems should require an understanding of the accompanying physicochemical changes caused by the increasing mobility of solute molecules during the heat treatment.[25] For example, heat-induced crystallization of a component salt in some buffer systems (e.g., sodium phosphate) significantly shift pH of the freeze-concentrated solutions and dried solids, and thus alters the stability of colyophilized proteins.[26,27] Reported phase separation of freeze-dried trehalose and dextran upon exposure to the higher temperature and humidity[28] suggested chances for similar component miscibility changes during the heat treatment of frozen solutions.

Frozen aqueous solutions containing nonreducing disaccharides (e.g., sucrose and trehalose) and polymers (PVP and dextran), which are popular as model systems that mimic the freeze-dried protein formulations and amorphous matrix solid dispersion formulations, were used to study the effect of the heat treatment on the solute miscibility in freeze-concentrated solutions and subsequently dried solids.[11] The word "heat treatment" rather than "annealing" is mainly used in the following text to simply describe the operation. The heat treatment of frozen aqueous solutions at temperatures just below T_g', which induces additional ice formation (devitrification), or post-lyophilization annealing were not addressed in this study.[29,30] Possible mechanisms of the physical changes and their relevance to the formulation qualities are discussed.

MATERIALS AND METHODS

Materials

All chemicals employed in this study were of analytical grade and were obtained from the following commercial sources: D-(+)-glucose, sucrose, D-(+)-trehalose dehydrate, PVP 10,000, PVP 29,000, and PVP 360,000 (Sigma Chemical, St. Louis, Missouri); dextran 40,000 (MP Biomedicals, Solon, Ohio); and maltotriose (Hayashibara Biochemical Laboratories, Okayama, Japan).

Thermal Analysis of Frozen Solutions and Freeze-Dried Solids

Thermal analysis of the frozen solutions and dried solids was performed by using a differential scanning calorimeter (DSC Q-10; TA Instruments, New Castle, Delaware) and Universal Analysis software (TA Instruments). Aliquots of aqueous solutions (10 μL) in aluminum cells were cooled from room temperature to −70°C at 10°C/min. The first heating scan of the frozen solution at 5°C/min was posed at varied temperatures (−25°C to −5°C, −5°C unless otherwise mentioned), and then maintained at the temperature for periods of various lengths (1–480 min, 30 min unless otherwise mentioned). After the sample solutions were cooled again to −70°C, the second heating scan was performed at a scanning rate of 5°C/min. Solids (~2 mg) lyophilized in aluminum DSC cells were used in the thermal analysis to reduce water vapor

absorption during the sample preparation. The cells were closed hermetically and then subjected to the thermal analysis from −20°C at 5°C/min under a nitrogen gas flow. The glass transition temperatures (T_g' and T_g) were obtained from the maximum inflection point of the discontinuities in the heat flow curves. The two-step heat flow changes observed in the second scan of some heat-treated frozen solutions were provisionally described as lower temperature ($T_g'_{2L}$) and higher temperature ($T_g'_{2H}$) transitions.

Freeze-Drying

A freeze-drier (FreeZone-6; Labconco, Kansas City, Missouri) was used for lyophilization. Aluminum thermal analysis hermetic pans (TA Instrument) filled with aqueous excipient solutions (10 μL) were placed inside of flat-bottom glass vials (13 mm in diameter; Nichiden-Rika Glass, Kobe, Japan). The vials containing the solution-filled DSC cells or larger volumes of aqueous solutions (1.0 mL, 21 mm diameter vial) transferred to the lyophilizer shelf were cooled to −36°C at 0.5°C/min, and then maintained at this temperature for 2 h before the primary drying process. Heat treatment of the frozen solutions was performed at −5°C for 1 h before the second cooling down to −36°C. The frozen solutions were dried under a vacuum (4.0 Pa), whereas the shelf temperature was maintained at −36°C for 24 h, −30°C for 6 h, −24°C for 6 h, and 35°C for 6 h. The shelf was heated at a rate of 0.2°C/min between the thermal steps. The vials were closed with rubber stoppers under a vacuum.

RESULTS AND DISCUSSION

Heat Treatment of Frozen Disaccharide and PVP Mixture Solutions

Frozen aqueous solutions containing varied concentration ratios of sucrose and PVP 29,000 (total 20%, w/w) were subjected to thermal analysis to examine the effect of the heat treatment (Fig. 1). Derivative thermograms of the frozen solutions obtained in the first heating scans (dotted lines) and the second heating scans (solid lines) after heat treatments at −5°C for 30 min showed peaks at T_g', where the step changes of the heat flow are observed in the original temperature scans. The single-solute frozen 20% sucrose and PVP 29,000 solutions presented T_g's at −33.9°C and −23.2°C, respectively, in the first scans. Smaller transitions at lower temperatures (sucrose: −45.6°C, PVP 29,000: −34.4°C) were also observed.[31,32] The heat treatment induced a small (1°C–2°C) upward shift of the main T_g's in the second heating scan, suggesting that further solute concentration occurred by means of additional ice crystallization in these frozen solutions.[29] The T_g' of the

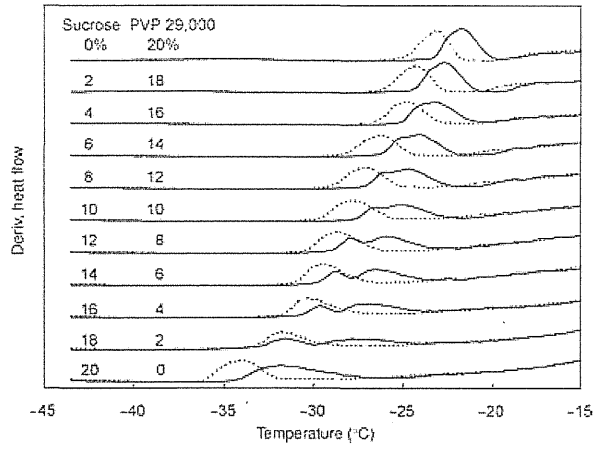

Figure 1. Derivative thermograms of frozen solutions (10 μL) containing sucrose and PVP 29,000 at varied concentration ratios obtained in the first heating scans from −70°C at 5°C/min (dotted lines) and in the second scans after a heat treatment at −5°C for 30 min (solid lines).

frozen sucrose solution became broader upon application of the heat treatment.

The frozen solutions containing both sucrose and PVP 29,000 (total: 20%, w/w) showed single T_g's in the first heating scans. The transition temperatures that moved between those of the component solutes suggested mixing of the solutes in the freeze-concentrated nonice phase. The heat treatment at −5°C for 30 min altered the shape and temperature of the T_g's differently, depending on the solute compositions. The single T_g's of PVP-rich frozen solutions shifted to higher temperatures (1°C–2°C) upon application of the heat treatment. The same heat treatment induced two-step changes of the heat flow in the frozen solutions containing higher concentration ratios of sucrose (e.g., 10%–18% sucrose): these changes appeared as two peaks in the derivative thermograms. These frozen solutions also showed much smaller thermal transitions at −50°C to −40°C (data not shown). The broad nature of these lower-temperature transitions prevented detailed analysis in this study.

The effect of the heat treatment temperature and time on the thermal properties of the frozen multisolute solutions was studied to further elucidate the physical changes that occurred. The frozen solutions containing 14% sucrose and 6% PVP 29,000 showed time-dependent splitting of the T_g' peak by the heat treatment at −5°C (Fig. 2). The broad but apparent two peaks observed after the longer heat treatment (10–480 min) strongly suggested the separation into two different transition temperature states rather than toward a particular single-T_g' state. Figure 3 shows the effect of the heat treatment temperatures (−25°C to −5°C) on the T_g's of frozen solutions

 DOI 10.1002/jps

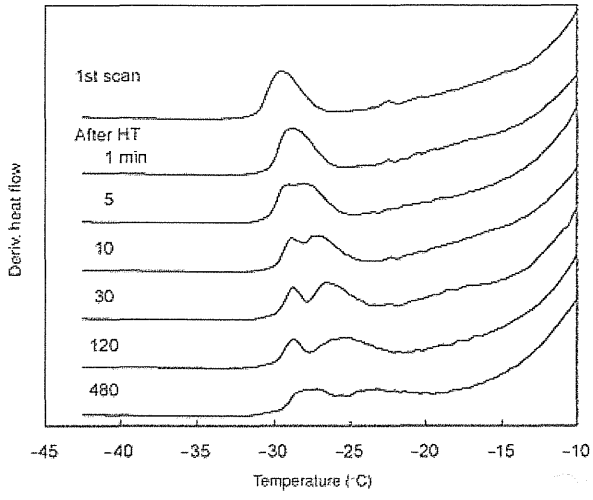

Figure 2. Derivative thermograms of frozen solutions (10 μL) containing 14% sucrose and 6% PVP 29,000 obtained in the first heating scans from −70°C at 5°C/min and in the second scans after heat treatments at −5°C for 1–480 min.

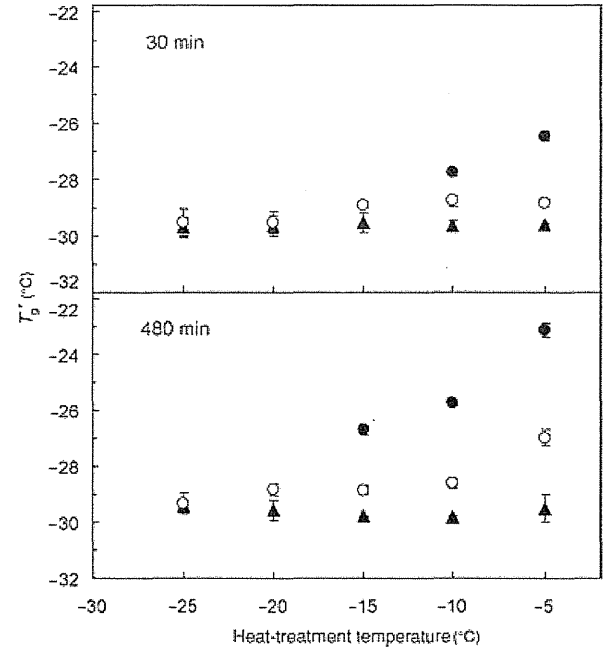

Figure 3. Effects of heat treatment temperatures (−25 to −5°C) on the T_g's of frozen solutions (10 μL) containing 14% sucrose and 6% PVP 29,000 obtained in the scans from −70°C at 5°C/min prior to (▲) and after (○,●) the heat treatment (30, 480 min, $n = 3$, average ± SD).

containing 14% sucrose and 6% PVP 29,000. The heat treatment at higher temperatures (−5°C and −10°C) induced faster splitting of the T_g' peak and an increased margin between the split peaks. Contrarily, the frozen solutions heat treated at lower temperatures (−20°C and −25°C) showed a single transition that was essentially equal to those obtained in the first scan. A longer time was required to induce the apparent T_g' splitting in the heat treatment at the intermediate temperature (−15°C). The heat treatment of the frozen mixture solution at a temperature just below the T_g' (e.g., −35°C, 480 min) resulted in exothermic drift of the thermogram at above the T_g' that suggested the relaxation of the system in the second heating scan (data not shown).[29]

Solutions containing varied total concentrations of sucrose and PVP 29,000 (7:3 weight concentration ratios) were also subjected to thermal analysis in order to study the effect of the heat treatment (Fig. 4). The T_g's obtained in the first scan did not depend largely on the total solute concentrations (5%–20%, w/w). The higher-concentration solutions showed a higher propensity for the T_g' splitting to occur upon the application of the heat treatment at −5°C. The two T_g's that were observed only after the longer heat treatment suggested slower phase separation in the lower-concentration solute mixture solutions (5% total, w/w). This trend was much different from that of the freeze concentration-induced phase separation of polymer mixtures that resulted in two T_g's in the first scan even for lower-concentration solutions.[16]

The frozen solutions containing various saccharides and polymers were subjected to thermal

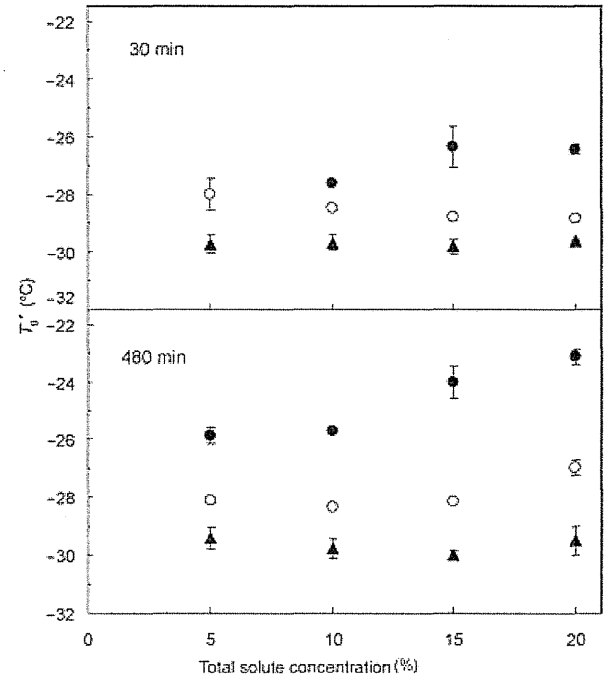

Figure 4. Effects of total solute concentrations on the transition temperatures (T_g's) of frozen solutions (10 μL) containing sucrose and PVP 29,000 at a 7:3 weight ratio scanned from −70°C prior to (▲) and after (○, ●) a heat treatment at −5°C (30, 480 min, $n = 3$, average ± SD).

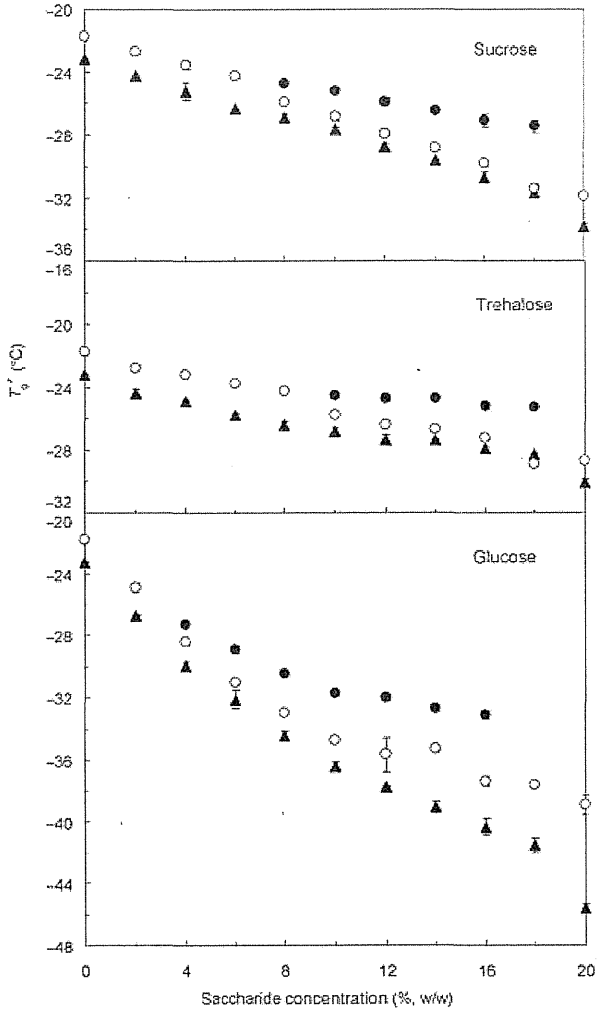

Figure 5. Transition temperatures (T_g's) of frozen solutions (10 μL) containing varied concentration ratios of low-molecular-weight saccharide and PVP 29,000 (total 20%, w/w). Symbols denote T_g's obtained in the heating scans prior to (▲) and after (○, ●) the heat treatment at −5°C for 30 min (n = 3, average ± SD).

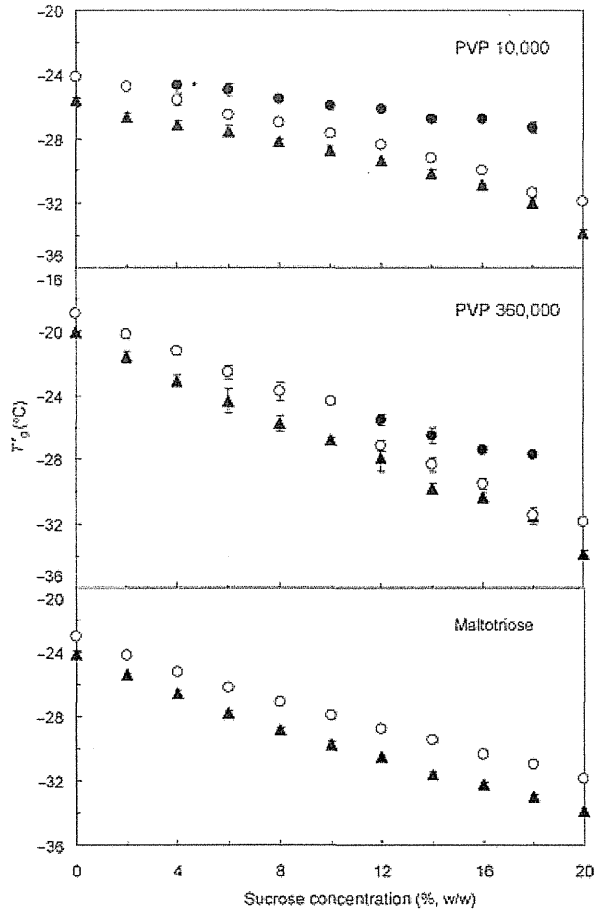

Figure 6. Transition temperatures (T_g's) of frozen solutions (10 μL) containing varied concentration ratios of sucrose and PVP or maltotriose (total 20%, w/w). Symbols denote T_g's obtained in the heating scans prior to (▲) and after (○, ●) the heat treatment at −5°C for 30 min (n = 3, average ± SD). *, two transitions were observed in two of three scans.

analysis to elucidate the effect of the heat treatment. The frozen solutions containing saccharide-rich mixtures of PVP 29,000 and disaccharides showed the splitting of the T_g' upon application of the heat treatment (−5°C, 30 min, Fig. 5). Contrarily, the single-solute and polymer-rich frozen solutions showed slight upward shifts of the single T_g's. The heat-treated frozen solutions containing glucose and PVP 29,000 showed two T_g's at wider concentration ratios. The effect of the heat treatment on the transition temperatures of the frozen solutions containing sucrose and varied-molecular-weight PVPs (PVP 10,000, 360,000) is shown in Figure 6. The frozen smaller PVP solution showed the T_g' at lower temperature.[33] The two T_g's were observed at wider concentration ratio in the heat-treated mixtures containing sucrose and smaller PVP molecules (10,000) compared with those containing larger PVP molecules (360,000). The figure also shows the T_g's of the frozen sucrose and maltotriose mixture solutions. The slight upward shift of the single T_g' that occurred upon the application of the heat treatment indicated further concentration of the miscible noncrystalline solutes at all concentration ratios.[34]

The splitting of T_g's should indicate the separation of the freeze-concentrated solutes into multiple phases that differ in their solute compositions upon the application of the heat treatment. This definition of the change, rather than the proposition that a two-step physical property change occurs in a miscible concentrated phase, was better supported by the observation of the T_g' split only in particular frozen solute-mixture solutions. The large effect of the heat treatment temperature and time on the

 DOI 10.1002/jps

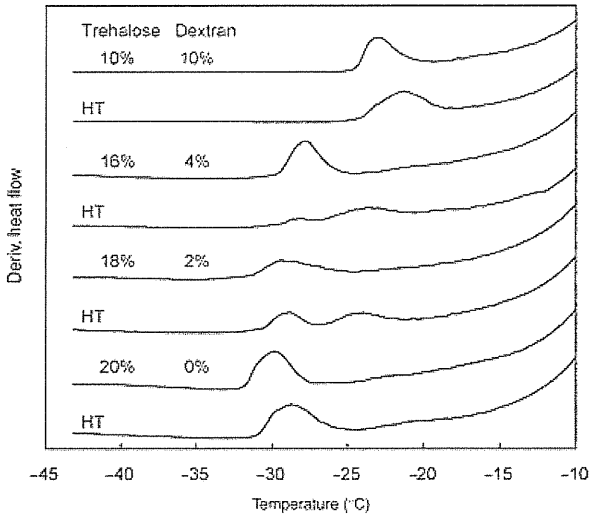

Figure 7. Derivative thermograms of frozen solutions (10 μL) containing varied concentration ratios of trehalose and dextran 40,000 obtained in the heating scans prior to and after the heat treatment at −5°C for 30 min.

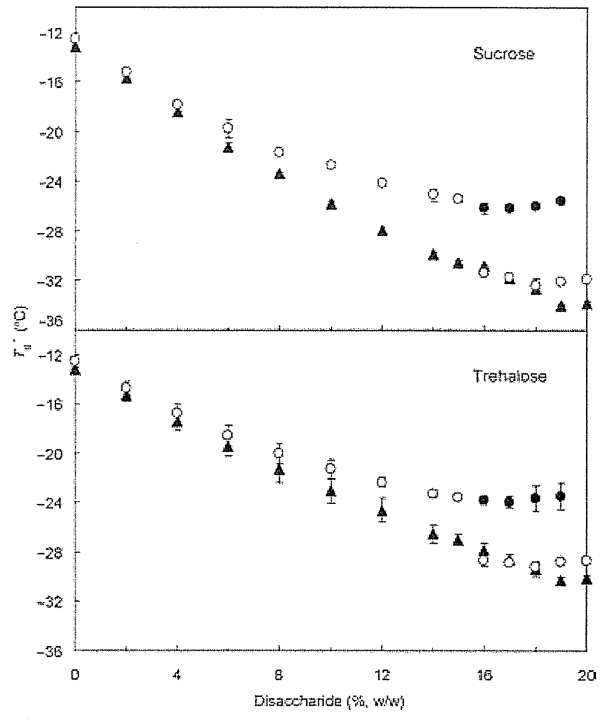

Figure 8. Transition temperatures (T_g's) of frozen solutions (10 μL) containing varied concentration ratios of disaccharide and dextran 40,000 (total 20%, w/w). Symbols denote T_g's obtained in the heating scans prior to (▲) and after (○, ●) the heat treatment at −5°C for 30 min (n = 3, average ± SD).

T_g' splitting strongly suggested that the increasing mobility of water and solute molecules helped to induce the phase separation. Solute compositions in the heat treatment-induced multiple freeze-concentrated phases were not clear from the transition temperatures in the PVP-containing systems.

Heat Treatment of Frozen Disaccharide and Dextran Mixture Solutions

Frozen solutions containing a disaccharide (trehalose and sucrose) and dextran 40,000 also showed a single T_g' in the heating scans prior to the heat treatment (Figure 7 and 8). Exposing the disaccharide-rich frozen mixture solution to a higher temperature (−5°C, 30 min) induced the splitting of the T_g', leading to two peaks in the derivative thermograms. The transition temperature profiles suggested solute compositions in the multiple freeze-concentrated phases of the heat-treated dextran-containing systems. The heat-treated frozen solutions containing 16%–19% trehalose showed their lower temperature transition ($T_g'_{2L}$) near the point of the single transition of the heat-treated frozen trehalose solution, suggesting changes of the concentrated disaccharide phase. The higher temperature transition ($T_g'_{2H}$) phase should contain certain concentration ratios of disaccharide and dextran. Contrarily, the slight upward shift of the single T_g's indicated further concentration of the solute mixture in the heat-treated frozen solutions containing higher concentrations of dextran. The heat treatment induced similar changes in the transition temperatures in the mixtures containing sucrose and dextran 40,000.

The effect of the heat treatment temperatures (−25°C to −5°C) on the T_g' of frozen solutions containing 18% trehalose and 2% dextran 40,000 is shown in Figure 9. Exposing the frozen solutions to higher temperatures (−5°C and −10°C) induced faster splitting of the T_g's. The frozen solution maintained a single T_g' upon the application of the heat treatment at a temperature just above T_g' (−25°C). The longer heat treatment (480 min) at the intermediate temperatures induced T_g' splitting (−20°C) or increased the margin between the two T_g' peaks (−15°C and −10°C). This result also indicates that higher solute mobility contributed to the phase separation of the multisolute frozen solutions. No changes that suggest the crystallization of trehalose were observed in these frozen mixture solutions.[35]

Some frozen solutions containing sucrose and a polymer were freeze-dried in the DSC cells with or without prior heat treatment at −5°C (60 min) to study the physical properties of the resulting solids. The heating scan of the sucrose solid that was freeze-dried without the heat treatment showed glass transition (T_g: 70.2°C), sucrose crystallization exotherm (onset at ~120°C), and sucrose crystal melting endotherm (~180°C, Fig. 10, some data not shown). Colyophilization with dextran 40,000 or PVP